

# ELSA: Efficient LLM-Centric Split Aggregation for Privacy-Aware Hierarchical Federated Learning over Resource-Constrained Edge Networks

Xiaohong Yang, Tong Xie, Minghui Liwang, Chikai Shang, Yang Lu, Zhenzhen Jiao, Liqun Fu, Seyyedali Hosseinalipour

## Abstract

Training large language models (LLMs) at the network edge faces fundamental challenges arising from device resource constraints, severe data heterogeneity, and heightened privacy risks. To address these, we propose ELSA (Efficient LLM-centric Split Aggregation), a novel framework that systematically integrates split learning (SL) and hierarchical federated learning (HFL) for distributed LLM fine-tuning over resource-constrained edge networks. ELSA introduces three key innovations. First, it employs a task-agnostic, behavior-aware client clustering mechanism that constructs semantic fingerprints using public probe inputs and symmetric KL divergence, further enhanced by prediction-consistency-based trust scoring and latency-aware edge assignment to jointly address data heterogeneity, client unreliability, and communication constraints. Second, it splits the LLM into three parts across clients and edge servers, with the cloud used only for adapter aggregation, enabling an effective balance between on-device computation cost and global convergence stability. Third, it incorporates a lightweight communication scheme based on computational sketches combined with semantic subspace orthogonal perturbation (SS-OP) to reduce communication overhead while mitigating privacy leakage during model exchanges. Experiments across diverse NLP tasks demonstrate that ELSA consistently outperforms state-of-the-art methods in terms of adaptability, convergence behavior, and robustness, establishing a scalable and privacy-aware solution for edge-side LLM fine-tuning under resource constraints.

## 1 Introduction

Large language models (LLMs) have demonstrated remarkable performance across diverse language tasks, and are typically adapted to real-world applications via fine-tuning [Luo *et al.*, 2025; Zhang *et al.*, 2025b; Liu and Zhao, 2026]. Nevertheless, deploying LLM fine-tuning directly on resource-constrained edge devices faces fundamental limitations in compute, memory, communication, and energy

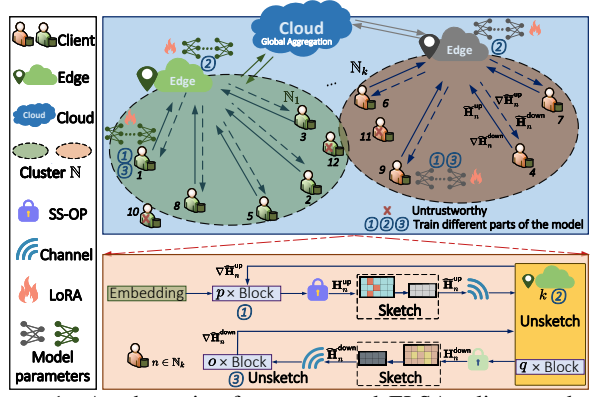


Figure 1: A schematic of our proposed ELSA: clients and edge servers collaboratively fine-tuning LLMs via LoRA, with activations compressed during transmission; the cloud globally aggregates the LoRA parameters.

[Farr *et al.*, 2025; Yang *et al.*, 2025a]. Moreover, data collected at the edge is inherently non-independent and identically distributed (non-IID), which exacerbates local model bias across edge devices. Together, these challenges highlight the need for a principled, architecture-aware distributed learning framework capable of enabling resource-efficient and robust LLM fine-tuning across edge devices [Liu *et al.*, 2022; Xu *et al.*, 2023; Mai *et al.*, 2024].

Federated learning (FL) offers a natural solution to the aforementioned challenges by enabling collaborative model training across geo-distributed edge devices with non-IID data [Yang *et al.*, 2025b; Chen *et al.*, 2025a]. However, as the scale of the system grows, requiring all edge devices to directly communicate with a single server can lead to severe congestion over backhaul links and impose substantial communication overhead. To alleviate this bottleneck, hierarchical federated learning (HFL) has emerged as an extension of FL [Chen *et al.*, 2025c; Lu *et al.*, 2024; Wu *et al.*, 2024]. While HFL improves scalability and reduces backhaul load, it largely assumes that full model updates can still be locally obtained and transmitted, an assumption that becomes increasingly untenable for LLMs due to their massive parameter sizes and memory footprints. These limitations motivate the incorporation of split learning (SL), which partitions the model across devices and servers, enabling edge devices to train only lightweight model segments locally while

offloading deeper, more resource-intensive components to computationally-capable network nodes (i.e., edge and cloud servers) [Lin *et al.*, 2024; Kim *et al.*, 2024]. Although the combination of HFL and SL is particularly promising for scalable and resource-efficient LLM fine-tuning at the network edge, a principled framework that jointly integrates these two paradigms for LLMs remains largely unexplored, motivating this work. Specifically, we propose ELSA (Efficient LLM-centric Split Aggregation), which aims to systematically investigate the potential of jointly integrating SL and HFL for LLM fine-tuning, forming a novel hybrid SL-HFL framework, entailing the following key contributions:

- We design a task-agnostic, behavior-aware hierarchical clustering mechanism. This strategy is further enhanced with (i) a trustworthiness score based on prediction consistency (to filter poisoned or noisy clients), and (ii) a latency-aware edge server assignment policy. In addition, we develop an SL-aware model segmentation strategy that explicitly leverages the heterogeneous capabilities of devices and edge servers.
- We introduce a model compression scheme based on computational sketches. Building on this design, we incorporate semantic subspace orthogonal perturbation (SS-OP) to preserve data privacy throughout the training process.
- Extensive evaluations on natural language processing (NLP) tasks, including text classification and information extraction, demonstrate that ELSA consistently outperforms state-of-the-art benchmarks.

## 2 Relate Work

### 2.1 FL-driven Fine-Tuning of LLMs over Edge Networks

FL has been recently explored as a promising paradigm for LLM fine-tuning in network edge environments. For example, [Qiao *et al.*, 2025] introduced an adaptive asynchronous accelerated FL for LLMs to enhance resource utilization efficiency and model accuracy in edge computing environments. [Liang *et al.*, 2023] designed FL-empowered collaborative training for bidirectional encoder representations from transformers (BERT) models and multi-scale convolutional neural networks (CNNs). Also, [Ding and Hu, 2024] facilitated multi-user collaborative training of LLMs by integrating FL with model parallelism strategies, while [Zhang *et al.*, 2025a] proposed a lightweight large-model-based joint multi-task multi-domain learning framework. Moreover, [Tang *et al.*, 2025] presented an FL-driven LLM fine-tuning malicious traffic detection method using BERT, and [Chen *et al.*, 2024] introduced a collaborative training framework for Transformer block classification based on FL.

The above works often overlook scalability bottlenecks in large edge networks as they rely on direct client-to-server communication that can cause congestion on backhaul links, exacerbated by heterogeneity and resource limits. While HFL alleviates this via intermediate aggregation for narrow models [Fang *et al.*, 2024; Sai *et al.*, 2025; Zhang *et al.*, 2025a], its

adaptation to LLM fine-tuning remains underexplored. Further, the massive size of LLMs demands a redesigned HFL framework, a gap that this work aims to address through the integration of SL.

### 2.2 Review of the Use of SL over Edge Networks

To address the challenges of LLM fine-tuning at the network edge under device resource constraints, two prevalent strategies are commonly adopted: (i) fine-tuning only a subset of LLM parameters using parameter-efficient methods such as low-rank adaptation (LoRA); and (ii) partitioning the model into multiple segments and distributing the training process across multiple computing nodes. Both strategies have recently attracted significant attention in the literature. For instance, [Tian and Yuan, 2025] proposed to partitioning the LLM into two segments for client-server collaborative training. [Ma *et al.*, 2025] proposed a fine-tuning framework for LLMs by strategically partitioning LLMs into device-side frozen layers and server-side, LoRA-enabled fine-tuning layers. [Wang *et al.*, 2023] introduced a lightweight mask-based segmentation learning framework for the collaborative fine-tuning of LLMs. [Cheng *et al.*, 2023] presented a distributed hybrid federated segmentation learning framework that leverages device-to-device (D2D) communications to aggregate edge resources for model training. [Tian *et al.*, 2022] designed a segmented learning framework to facilitate the collaborative training of BERT models.

Although the above studies have advanced LLM fine-tuning, they have largely neglected the communication costs incurred during conventional FL: they do not consider LLM fine-tuning under HFL architectures, which entail a better scalability and backhaul link load. In addition, privacy vulnerabilities arising from the joint use of HFL and SL in LLM fine-tuning, particularly those related to information leakage through shared model updates, remain largely unexplored.

## 3 Proposed Method

### 3.1 Problem Formulation

We consider distributed learning through an HFL architecture, where the system consists of a cloud server, multiple edge servers  $\mathcal{K} = \{1, \dots, k, \dots, K\}$ , and a set of clients  $\mathcal{N} = \{1, \dots, n, \dots, N\}$ , as illustrated in the upper right portion of Fig. 1. Each client  $n$  owns a local dataset  $\mathcal{D}_n = \{(\mathbf{x}_j, y_j) | 1 \leq j \leq |\mathcal{D}_n|\}$ , where  $\mathbf{x}_j$  and  $y_j$  refer to the feature vector and the label of the  $j^{\text{th}}$  local data point, respectively. Subsequently, given a pre-trained LLM with fixed backbone parameters  $w^{\text{LLM}}$  and the trainable fine-tuning parameter  $\theta$ , the loss function for a data sample  $(\mathbf{x}_j, y_j)$  is defined via the task specific loss (e.g., cross entropy for classification):

$$f(\mathbf{x}_j, y_j; w^{\text{LLM}}, \theta) = \mathcal{L}_{\text{task}}(\psi(\mathbf{x}_j; w^{\text{LLM}}, \theta), y_j) \quad (1)$$

where  $\psi(\cdot)$  is the representation output of LLM. Collectively, the optimization objective to minimize the global loss function across all participating clients, is given by:

$$\operatorname{argmin}_{\theta} \widetilde{F}(\theta) = \sum_{n=1}^N \frac{|\mathcal{D}_n|}{|\mathcal{D}|} F_n(\theta), \quad (2)$$

where  $|\mathcal{D}| = \sum_{n=1}^N |\mathcal{D}_n|$ , and

$$F_n(\theta) = \frac{1}{|\mathcal{D}_n|} \sum_{(\mathbf{x}_j, y_j) \in \mathcal{D}_n} f(\mathbf{x}_j, y_j; w^{\text{LLM}}, \theta). \quad (3)$$

### 3.2 HFL with Tripartite Split Training

In the following, we first introduce a client clustering strategy based on Kullback–Leibler divergence (KLD) to address data heterogeneity and unreliable trustworthiness and communications across clients. Then, we detail the end-to-end workflow of LLM partitioning and collaborative training across clients. Finally, we present a compression framework aimed at simultaneously enhancing communication efficiency and safe guarding the data privacy during training.

#### Behavior-aware Hierarchical Clustering

Prior FL/HFL methods cluster clients via KL divergence on label distributions [Rahad *et al.*, 2025; Yang *et al.*, 2025c] to mitigate the adverse effects of non-IID data, under the assumption that similar class proportions imply compatible optimization landscapes, a reasonable approximation for vision tasks with CNNs but ill-suited for LLMs. In distributed LLM fine-tuning, (i) downstream tasks lack a shared label space (e.g., classification vs. summarization), and (ii) heterogeneity arises from semantic/behavioral divergence, how local models interpret identical inputs, not just class imbalance. Moreover, real-world HFL must handle unreliable clients (e.g., poisoned data) and unstable connectivity. To address these gaps, our framework combines probe-based behavioral fingerprints, prediction-consistency trust scores, and latency-aware client–server assignment to enable robust, scalable HFL for LLMs. Subsequently, we formalize our approach in four steps:

**Step 1: Construction of a Public Probe Set.** We construct a lightweight public probe set  $\mathcal{P} = \{\mathbf{x}^{(1)}, \dots, \mathbf{x}^{(Q)}\}$  from open benchmarks (e.g., GLUE [Wang *et al.*, 2019]), distributed to all clients as a common reference for privacy-preserving behavioral evaluation.

**Step 2: Task-Agnostic Behavioral Fingerprint Extraction.** For each client  $n$ , we feed every probe input  $\mathbf{x}^{(j)} \in \mathcal{P}$  into its locally fine-tuned LLM (e.g., BERT) and extract the contextual representation of the [CLS] token, a standard sentence-level embedding used across transformer-based LLMs, denoted by  $\mathbf{T}_n^j \in \mathbb{R}^{D^{\text{hidden}}}$ , where  $D^{\text{hidden}}$  represents the hidden dimension. To obtain a unified-dimension, task-agnostic profile that is invariant to downstream task head structures, we model the client’s behavioral fingerprint as a multivariate Gaussian distribution:  $R_n = \tilde{\mathcal{N}}(\boldsymbol{\mu}_n, \Sigma_n)$ , where  $\boldsymbol{\mu}_n = \frac{1}{Q} \sum_{j=1}^Q \mathbf{T}_n^{(j)}$  and  $\Sigma_n = \frac{1}{Q} \sum_{j=1}^Q (\mathbf{T}_n^{(j)} - \boldsymbol{\mu}_n)(\mathbf{T}_n^{(j)} - \boldsymbol{\mu}_n)^\top$  are the empirical mean and covariance of the client’s [CLS] embeddings over the probe set.

**Step 3: Symmetric KL Divergence for Behavioral Discrepancy.** We quantify the data heterogeneity between clients  $n$  and  $n'$  via the symmetrized KL divergence between their Gaussian fingerprints:

$$\mathcal{R}(n, n') = \text{KL}(R_n \| R_n') + \text{KL}(R_n' \| R_n), \quad (4)$$

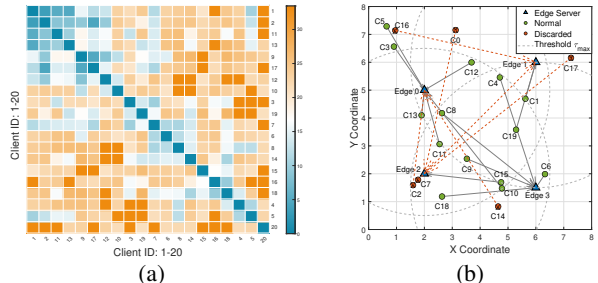


Figure 2: Client behavioral heterogeneity and clustering outcome in a 20-client network. Left:  $20 \times 20$  pairwise KL divergence matrix  $\mathcal{R}(n, n')$  across all clients. Right: final client-server association mapping.

where the closed-form KL between multivariate Gaussians is given by

$$\begin{aligned} \text{KL}(\tilde{\mathcal{N}}_n \| \tilde{\mathcal{N}}_{n'}) &= \frac{1}{2} \left[ \text{tr}(\boldsymbol{\Sigma}_{n'}^{-1} \boldsymbol{\Sigma}_n) - D^{\text{hidden}} + \ln \frac{|\boldsymbol{\Sigma}_{n'}|}{|\boldsymbol{\Sigma}_n|} \right. \\ &\quad \left. + (\boldsymbol{\mu}_{n'} - \boldsymbol{\mu}_n)^\top \boldsymbol{\Sigma}_{n'}^{-1} (\boldsymbol{\mu}_{n'} - \boldsymbol{\mu}_n) \right]. \end{aligned} \quad (5)$$

**Step 4: Trust and Communication-Aware Client Clustering.** We integrate trustworthiness and communication feasibility into a unified client clustering framework. Specifically, we first compute a *trustworthiness score* for each client  $n$ :

$$w_n^{\text{trust}} = \exp \left( - \underbrace{\frac{1}{Q} \sum_{j=1}^Q \frac{1}{\|\mathbf{T}_n^{(j)}\|_2}}_{\text{inverse confidence}} - \underbrace{\frac{1}{N-1} \sum_{n' \neq n} \mathcal{R}(n, n')}_{\text{mean behavioral divergence } \bar{\mathcal{R}}_n} \right),$$

where  $\frac{1}{\|\mathbf{T}_n^{(j)}\|_2}$  is the inverse confidence of its [CLS] embeddings across  $\mathcal{P}$ . Intuitively, a client with low prediction entropy (high confidence) and low divergence from peers (consistent behavior) receives a high trust score. We then define the *communication-feasible edge server set* for each client  $n$ :  $\mathcal{E}_n = \{k \mid \tau_{n,k} \leq \tau_{\max}, k \in \mathcal{K}\}$ , where  $\tau_{n,k}$  is the round-trip latency between client  $n$  and edge server  $k$ , and  $\tau_{\max}$  is a system-defined threshold (e.g., 200 ms). We finally construct a *communication-constrained client partition* through a three-stage process: (i) For each edge server  $k$ , we define its candidate client set as  $\mathcal{C}_k = \{n \mid k \in \mathcal{E}_n\}$ . (ii) Within each  $\mathcal{C}_k$ , perform spectral clustering using a trust-weighted affinity matrix:

$$\mathbf{A}_{n,n'}^{(k)} = w_n^{\text{trust}} \cdot w_{n'}^{\text{trust}} \cdot \exp(-\gamma \cdot \mathcal{R}(n, n')), \quad \forall n, n' \in \mathcal{C}_k,$$

where  $\gamma > 0$  controls the sensitivity to behavioral divergence. (iii) For each resulting cluster  $\mathbb{N}_k \subseteq \mathcal{C}_k$ , compute its average trust score  $\bar{w}_k^{\text{trust}} = \frac{1}{|\mathbb{N}_k|} \sum_{n \in \mathbb{N}_k} w_n^{\text{trust}}$ . If  $\bar{w}_k < w_{\min}$  (a trust threshold), either merge  $\mathbb{N}_k$  into the nearest high-trust cluster. Finally, the final grouping  $\{\mathbb{N}_k\}_{k=1}^K$  ensures clusters are behaviorally coherent, robust to polluted data, and assigned to reliably connected edge servers, enabling stable and deployable hierarchical aggregation.

To facilitate understanding, in Fig. 2, we consider a network with 20 clients with the local dataset of the clients

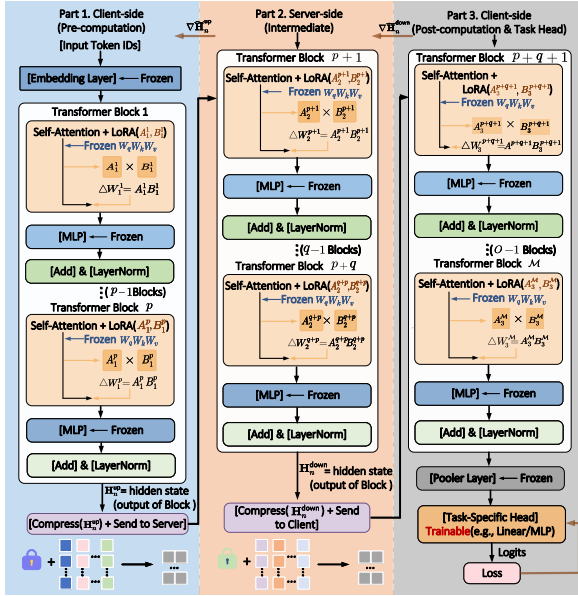


Figure 3: Breakdown of ELSA: client trains Part 1, sends compressed activations to edge for Part 2, which then feeds into Part 3 on client. Gradients flow backward symmetrically ( $\nabla \tilde{\mathbf{H}}_n^{\text{down}} \rightarrow$  Edge,  $\nabla \tilde{\mathbf{H}}_n^{\text{up}} \rightarrow$  Client), completing one round.

are formed via distributing the SQuAD dataset using Dirichlet distribution with parameter  $\hat{\alpha} = 0.1$ . Fig. 2(a) shows a heatmap of pairwise KLD ( $\mathcal{R}(n, n')$ ) visualizing data distribution shifts; Fig. 2(b) displays the final client clustering (client–server assignment). Only in-range, high-trust clients (green circles, ‘Normal’) participate in edge-level aggregation; others (marked ‘X’) are excluded as untrustworthy or out-of-range.

### Model Splitting and Collaborative Training

The tripartite model segmentation in ELSA, where both the initial (Part 1) and final (Part 3) segments reside on the client, and the intermediate transformer blocks (Part 2) are offloaded to the edge server, is designed to jointly ensure privacy, label confidentiality, and computational feasibility. By keeping the embedding layer and task-specific head on-device, sensitive data (input tokens, labels, and predictions) never leave the client, eliminating label leakage and mitigating reconstruction attacks on embeddings or logits. In Fig. 3, we partition a LLM architecture (e.g., BERT) with  $\mathcal{M}$  transformer blocks into three parts. Only low-rank adapter parameters  $\theta = [\theta_1, \theta_2, \theta_3]$  (i.e.,  $(A_1^1, B_1^1), \dots, (A_3^M, B_3^M)$ ) forming the adapters, where  $\|\theta\| \in \mathbb{R}^{\mathcal{M}} (\mathcal{M} \ll D)$  within each attention module and the lightweight task head—are trainable, ensuring minimal communication and memory overhead.

Each client  $n \in \mathbb{N}_k$  within the coverage edge server  $k$ , feed-forwards its data through Part 1 of its model, generating a hidden layer state, defined as

$$\mathbf{H}_n^{\text{up}} = [h_{n,1}^{\text{up}}, \dots, h_{n,d}^{\text{up}}, \dots, h_{n,D}^{\text{up}}] \in \mathbb{R}^D \Big|_{f_{\text{embed}}(x; \theta_1) \rightarrow f_{1 \sim p}}, \quad (6)$$

where  $h_{n,d}^{\text{up}}$  is the  $d$ -th component of  $\mathbf{H}_n^{\text{up}}$ ,  $f_{\text{embed}}(x)$  denotes the embedding layer of the LLM, and  $f_{1 \sim p}$  represents the sequential feed-forward through transformer block 1 to block  $p$  at the client. To mitigate privacy risks and communication cost, the client compresses  $\mathbf{H}_n^{\text{up}}$  via sketching and sends

the compressed representation (i.e.,  $\tilde{\mathbf{H}}_n^{\text{up}}$ ) along with attention mask  $\mathcal{A}_n$  to the edge server. The server reconstructs  $\tilde{\mathbf{H}}_n^{\text{up}}$  and processes it through Part 2, defined as

$$\mathbf{H}_n^{\text{down}} = [h_{n,1}^{\text{down}}, \dots, h_{n,d}^{\text{down}}, \dots, h_{n,D}^{\text{down}}] \in \mathbb{R}^D \Big|_{f_{p+1 \sim p+q}(\tilde{\mathbf{H}}_n^{\text{up}}, \mathcal{A}_n; \theta_2)}, \quad (7)$$

where  $h_{n,d}^{\text{down}}$  is the  $d$ -th component of  $\mathbf{H}_n^{\text{down}}$  and  $f_{p+1 \sim p+q}(\cdot)$  denotes sequential feed-forward through transformer blocks  $p$  to  $p+q$ . Then,  $\mathbf{H}_n^{\text{down}}$  will be compressed into  $\tilde{\mathbf{H}}_n^{\text{down}}$  and sent to the client. Next, the latest  $o$  model segments on client-side perform computations to obtain logits  $\mathcal{Z}$  and loss value, which triggers gradient backpropagation; mathematically,

$$\mathcal{Z} = f_{p+q+1 \sim \mathcal{M}}(\tilde{\mathbf{H}}_n^{\text{down}}, \mathcal{A}_n; \theta_3), \quad (8)$$

$$\mathbb{L} = \mathcal{F}_{\text{loss}}(f_{\text{out}}(\mathcal{Z}, y)), \quad (9)$$

where  $f_{p+q+1 \sim \mathcal{M}}(\cdot)$  denotes sequential feed-forward through transformer blocks  $p+q$  to  $p+q+o$ ,  $f_{\text{out}}(\cdot)$  is the output layer of the model,  $y$  is the targeting sentences and  $\mathcal{F}_{\text{loss}}(\cdot)$  denotes the loss function.

While client–edge collaboration improves training efficiency, the restricted representational power of isolated local updates can compromise global model expressiveness. To mitigate this, we fix  $\varrho$  collaborative training rounds each edge server  $k$  uploads its refined adapter parameters to the cloud for global aggregation, weighted by (i) the internal behavioral coherence of its client group, and (ii) the aggregated trustworthiness of the participating clients. Specifically, we define:  $\alpha_k = \frac{1}{1 + \overline{\mathcal{R}}_k} \times \bar{w}_k^{\text{trust}}$ , where  $\overline{\mathcal{R}}_k = \frac{1}{|\mathbb{N}_k|(|\mathbb{N}_k| - 1)} \sum_{n \neq n' \in \mathbb{N}_k} \mathcal{R}(n, n')$  is the average pairwise symmetric KLD among clients in  $\mathbb{N}_k$ . We normalize the weights as  $\tilde{\alpha}_k = \frac{\alpha_k}{\sum_{k=1}^K \alpha_k}$  and compute the global model:  $\theta_g = \sum_{k=1}^K \tilde{\alpha}_k \theta_{g,k}$ , where  $\theta_{g,k}$  denotes the adapter parameters from edge server  $k$  after its local collaborative training in the  $g^{\text{th}}$  round. Training terminates when consecutive global models satisfy  $\|\theta_g - \theta_{g-1}\|_2 \leq \xi$ , with  $\xi > 0$  a small convergence threshold (e.g., G).

### Layered Compression for Secure and Efficient Communications

To jointly reduce communication overhead and prevent privacy leakage during client–edge exchanges, we propose a semantic subspace orthogonal perturbation (SS-OP) mechanism based on computational sketches, designed to preserve semantic fidelity in model updates. Each client  $n$  first collects a matrix  $\mathbf{J}_n \in \mathbb{R}^{Q \times D^{\text{hidden}}}$ , denoting the matrix of  $\mathbf{Q}$  (e.g., [CLS] vectors) from recent probe or training inputs. Instead of applying a global orthogonal transform, it identifies its dominant semantic subspace via truncated SVD (or power iteration) to extract the top- $r$  principal components.

$$\mathbf{U}_n = \text{Top}_r(\text{SVD}(\mathbf{J}_n)) \in \mathbb{R}^{D^{\text{hidden}} \times r}, \quad (10)$$

where  $\mathbf{U}_n^T \mathbf{U}_n = \mathbf{I}_r$  spans the most informative semantic directions. Next, a client-specific random orthogonal matrix  $\mathbf{V}_n \in \mathbb{R}^{r \times r}$  is generated by QR decomposition of a pseudo-random Gaussian matrix seeded from the client ID and a pre-shared salt:  $\mathbf{V}_n = \text{QR}(\Phi(n))$ , where  $[\Phi(n)]_{i,j} \sim \tilde{\mathcal{N}}(0, 1)$

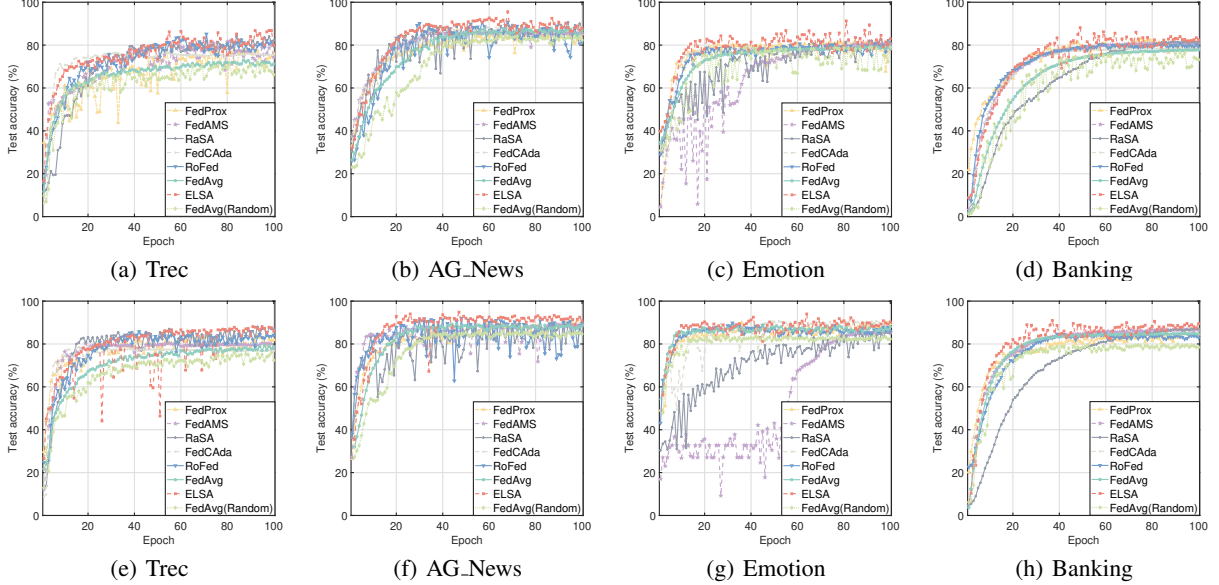


Figure 4: Test performance comparison across TC datasets under two levels of data heterogeneity: (a)–(d) correspond to  $\hat{\alpha} = 0.1$ , while (e)–(h) use  $\hat{\alpha} = 0.2$ .

Method	Data Setting $\hat{\alpha} = 0.1$				Data Setting $\hat{\alpha} = 0.2$			
	RTE Acc.	CB Acc.	MultiRC F1/EM	SQuAD F1/EM	RTE Acc.	CB Acc.	MultiRC F1/EM	SQuAD F1/EM
FedAvg	79.21	80.23	79.61/50.17	76.92/87.06	79.91	81.03	79.96/52.03	77.22/87.72
FedProx	78.92	82.14	80.68/49.19	78.33/ <b>87.31</b>	79.54	83.62	81.33/50.02	79.01/87.70
FedAMs	80.13	79.82	81.44/51.33	77.66/86.21	81.22	82.38	81.76/52.05	78.02/87.05
RaSA	78.92	81.24	79.55/51.27	78.38/86.79	80.53	83.24	80.62/52.08	78.99/86.95
FedCAda	79.23	82.66	79.81/51.39	78.52/86.45	81.31	84.23	80.12/52.41	80.03/87.29
RoFed	79.18	82.71	80.22/51.09	78.50/86.55	82.33	83.19	82.19/52.32	79.33/87.16
FedAvg (Random)	78.48	79.26	78.23/48.29	75.33/85.66	79.03	79.77	79.11/49.06	76.52/85.98
<b>ELSA (Ours)</b>	<b>80.93</b>	<b>83.93</b>	<b>81.78/52.06</b>	<b>79.24/87.17</b>	<b>83.13</b>	<b>84.99</b>	<b>82.72/53.16</b>	<b>80.44/88.04</b>
<i>Gain</i>	+0.80	+7.22	+0.34/+0.67	+0.72/-0.14	+0.82	+0.76	+0.63/+0.75	+0.41/+0.32

*Note:* Values are formatted as ‘performance / improve vs. best baseline’.

Table 1: Performance comparison on four NLP tasks under different  $\hat{\alpha}$  (0.1 and 0.2). Acc. (%) is reported for RTE and CB, while F1/EM is reported for MultiRC and SQuAD.

with  $\text{seed}_n = \text{Hash}(s \parallel n)$ , and  $s$  is a pre-shared salt value. The full perturbation matrix is then constructed as:

$$\mathcal{Q}_n = \mathbf{U}_n \mathbf{V}_n \mathbf{U}_n^\top + (\mathbf{I}_{D^{\text{hidden}}} - \mathbf{U}_n \mathbf{U}_n^\top). \quad (11)$$

This matrix is orthogonal ( $\mathcal{Q}_n^\top \mathcal{Q}_n = \mathbf{I}_{D^{\text{hidden}}}$ ) and performs a random rotation *only within the semantic subspace*, leaving the orthogonal complement unchanged. This design ensures privacy (via secret-seeded orthogonal perturbation), exact gradient flow (due to orthogonality), and structural compatibility (by preserving inactive subspace dimensions). The uploaded hidden state is then computed as  $\mathbf{H}_n^{\text{up}} = \mathcal{Q}_n \mathbf{H}_n^{\text{up}}$ , which is compressed into a  $Y \times Z$  dimensional sketch matrix  $U$  using  $Y$  independent hash functions, where  $Z \ll D$ . Specifically, each sketch element can be calculated as:

$$U_{n,[j,k]} = \sum_{d:h_{n,j}(d)=u} \text{sign}_j(d) \cdot h_{n,d}^{\text{up}}, \quad (12)$$

where  $u \in \{1, 2, \dots, Z\}$  represents the column index of sketch matrix  $U$  and  $\text{sign}_{j:1 \leq j \leq Y} : D \rightarrow \{+1, -1\}$  denotes  $Y$  pairwise independent sign hash functions. Besides, we define the compression ratio throughout the entire transmission process as  $\rho = D/(YZ)$ . At the edge, we recover the original hidden

Method	AG_News	Banking	Emotion	Trec	RTE	CB	MultiRC	SQuAD
Vanilla Model	10.51	6.01	7.51	3.38	14.41	18.02	39.64	36.93
FedProx	3.65	1.97	2.29	1.04	4.65	5.72	13.73	13.08
FedAMs	3.57	1.99	2.01	1.00	4.58	6.24	14.58	14.16
RaSA	3.53	1.93	2.43	0.98	4.79	6.58	15.73	13.76
FedCAda	3.43	2.32	2.36	0.95	4.72	6.15	14.30	13.30
RoFed	3.36	1.89	2.32	0.97	4.43	6.01	13.44	13.08
FedAvg	3.79	2.14	2.32	1.07	4.58	6.29	14.87	13.94
FedAvg (Random)	3.93	2.22	2.50	1.09	5.00	7.15	16.87	14.58
<b>ELSA (Ours)</b>	<b>3.22/-0.14</b>	<b>1.86/-0.03</b>	<b>2.25/-0.04</b>	<b>0.89/-0.06</b>	<b>4.29/-0.14</b>	<b>5.43/-0.29</b>	<b>13.15/-0.29</b>	<b>12.23/-0.85</b>

*Note:* Values are formatted as ‘time / reduction vs. best baseline’.

Table 2: Comparison of the total communication time to reach target performance across different methods ( $\times 10^3$  s).

layer information based on the received  $U_{n,[j,k]}$  as follows:

$$\tilde{\mathbf{H}}_n^{\text{up}} = \text{Median}_{1 \leq j \leq Y} \{ \text{sign}_j(d) \cdot U_{n,[j,h_{n,j}(d)]} \}, \quad (13)$$

where  $\text{Median}(\cdot)$  is the median of all approximated values.

### Communication Modeling

In ELSA, each global iteration involves  $\varrho$  client–edge collaborative rounds and one edge-to-cloud LoRA upload (i.e.,  $|\theta^{\text{LoRA}}|$ ). The total communication overhead in the  $g^{\text{th}}$  global round is

$$C_g = \underbrace{\frac{2\varrho\zeta\mu D^{\text{hidden}}}{\rho} \sum_{k=1}^K \sum_{n \in \mathbb{N}_k} B_n}_{\text{Client} \leftrightarrow \text{Edge}} + \underbrace{K \cdot |\theta^{\text{LoRA}}|}_{\text{Edge} \rightarrow \text{Cloud}}, \quad (14)$$

where  $\zeta$  is the byte size per floating-point parameter (e.g., 4 for FP32),  $\mu$  the input sequence length,  $B_n$  the average mini-batch size of client  $n$ . Furthermore, the per-client communication time is  $\mathcal{T}_{g,n} = \frac{2\varrho B_n \mu \zeta D^{\text{hidden}}/\rho}{\mathcal{B}_{\text{eff}}}$ , where  $\mathcal{B}_{\text{eff}}$  represents the effective bandwidth (in bytes/second). Subsequently, the total communication time until convergence is given by

$$T_{\text{total}} \approx G \times \max_{n \in \mathbb{N}_k, k \in \mathcal{K}} (\mathcal{T}_{g,n}), \quad (15)$$

where  $G$  is the number of global iterations (epochs) required to satisfy the convergence criterion.

### 3.3 Convergence Analysis of ELSA

**Theorem 1.** Let  $\eta = \frac{1}{\mathcal{L}\sqrt{G}}$ , the sequence of global adapter parameters  $\{\theta_g\}_{g=0}^{G-1}$  generated by ELSA satisfies:

$$\frac{1}{G} \sum_{g=0}^{G-1} \mathbb{E} \left[ \left\| \nabla \tilde{F}(\theta_g) \right\|^2 \right] \leq \underbrace{\frac{4\mathcal{L}(\tilde{F}(\theta_0) - \tilde{F}^*)}{\sqrt{G}}}_{\text{optimization error}} + \underbrace{\frac{\sigma_{\text{local}}^2}{\sqrt{G}}}_{\text{vanishing noise}} + \underbrace{\frac{\sigma_2^2}{\sqrt{G}}}_{\text{non-IID bias}},$$

where  $\tilde{F}^* = \min_{\theta} \tilde{F}(\theta)$  denotes the optimal value of the global objective, and please see proof in Appendix.

## 4 Experiments and Evaluations

In the following, we aim to evaluate the proposed ELSA framework with respect to two key research questions:

- How does ELSA perform compared to existing methods?
- How do various hyperparameters affect ELSA’s performance, and how can their optimal values be determined?

### 4.1 Experimental Setup

**Datasets:** We consider eight diverse datasets spanning various NLP tasks: (i) *Text Classification (TC)*: *Trec*, *AG\_News*, *Emotion*, and *Banking77*, covering question, news, sentiment, and fine-grained intent classification [Li and Roth, 2002; Zhang et al., 2015; Oluwatobi and Erik, 2020]; (ii) *Natural Language Inference (NLI)*: *RTE* and *CB*, which involve premise-hypothesis entailment; *MultiRC* and *SQuAD*, representing multi-sentence reading comprehension and extractive question answering tasks respectively [Wang et al., 2019; Rajpurkar et al., 2016].

**Baselines:** We evaluate and compare the performance of FedProx [Li et al., 2020], FedAMS [Wang et al., 2022], RaSA [Wang et al., 2025], FedCAda [Zhou et al., 2025], RoFed [Wang et al., 2026] and FedAvg [McMahan et al., 2017]. Additionally, we also study the performance of FedAvg under randomly selected client conditions (i.e., FedAvg(Random)).

**Parameters settings:** We deploy 20 clients and 4 edge servers in an 8 km  $\times$  8 km area (Fig. 2(b)), and 4 clients are randomly selected to inject mislabeled samples, simulating unreliable data. We adopt BERT-base-uncased as the LLM architecture (12 Transformer blocks, a hidden dimension of 768, and 12 attention heads, totaling approximately 110 million parameters [Tang et al., 2025; Tian et al., 2022]). Data heterogeneity combines: *Quantity Skew*: each client  $n$  allocates a local subset  $\mathcal{D}_n$ , with the size  $|\mathcal{D}_n|$  proportional to a performance factor  $\chi_n = \frac{n+1}{\Omega_k}$ , where  $\Omega_k$  denotes the overall samples related to edge  $k$ ; *Label Distribution Skew*: class imbalance drawn from Dirichlet distribution  $\text{Dir}(\hat{\alpha})$  with  $\hat{\alpha} = \{0.1, 0.2\}$  [Gao et al., 2022].

	AG_News	Banking	Emotion	Trec	RTE	CB	MultiRC	SQuAD	Avg.
	Acc.	Acc.y	Acc.	Acc.	Acc.	Acc.	F1/EM	F1/EM	
$\rho = 2.1$	92.33	86.34	85.22	83.33	84.24	84.18	82.45/53.12	85.66/87.88	
Co. Be.	1.67	1.81	1.66	1.82	1.65	1.26	1.46	1.29	<b>1.63</b>
$\rho = 3.3$	91.08	84.21	85.02	83.08	83.18	84.03	81.87/53.01	84.13/87.48	
Co. Be.	2.98	2.68	2.77	2.68	2.73	2.01	2.45	2.26	<b>2.57</b>
$\rho = 6.4$	86.33	81.03	81.11	81.15	80.25	81.36	81.37/51.71	77.13/86.52	
Co. Be.	3.65	3.84	3.39	4.85	4.46	3.28	3.86	3.12	<b>3.81</b>
$\rho = 8.4$	83.22	75.46	78.22	74.66	75.97	73.66	73.34/47.22	76.22/82.11	
Co. Be.	3.39	4.27	4.33	5.56	3.45	2.24	2.46	3.80	<b>3.69</b>
$\rho = 11.8$	78.03	70.31	72.84	71.81	72.25	68.34	68.19/43.18	72.55/80.06	
Co. Be.	3.98	4.57	4.72	5.82	4.98	5.90	3.77	3.87	<b>4.70</b>

Table 3: Sensitivity of ELSA to compression ratio  $\rho$ : performance and communication benefit.

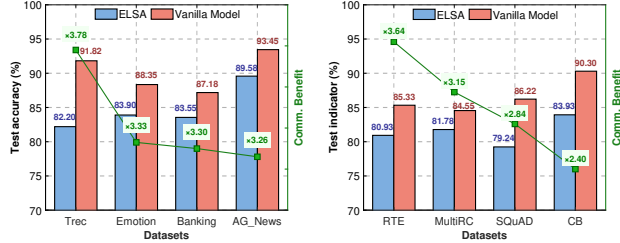
### 4.2 Evaluation of Learning Efficiency and Model Performance

To evaluate training performance, we prioritize convergence rate on TC datasets to assess communication efficiency, and steady-state metrics (Acc., F1, EM) on NLI tasks that require complex semantic reasoning. This ensures that we can capture both learning efficiency and final representational capacity [Tang et al., 2025; Wang et al., 2026]. As shown in Fig. 4, under quantity-based heterogeneity, ELSA exhibits superior convergence across all TC datasets. Though its initial speed is occasionally slower (e.g., Fig. 4(a), (d), (e)), it consistently reaches a higher final accuracy, indicating better optimization stability. Table 1 shows ELSA achieves state-of-the-art steady-state performance on NLI tasks (e.g., 80.93% on RTE and 81.78% on MultiRC, lagging only slightly behind FedProx on SQuAD (-0.14% EM)). This consistent gain across tasks and heterogeneity levels underscores the robustness of ELSA’s dual-stage semantic consistency framework in practical edge settings. During clustering, behavior-aware fingerprints capture clients’ update patterns to group semantically similar participants, while during aggregation, coherence- and trust-weighted fusion dynamically calibrates contributions based on both feature alignment and historical reliability. Additionally, the observed performance gap between FedAvg and FedAvg (Random) across datasets stems from the latter’s vulnerability to unverified clients, further validating the critical necessity of our trust-aware client clustering and aggregation strategy.

### 4.3 Evaluation of Communication Costs and Transmission Efficiency

In the following, we evaluate ELSA by analyzing its communication-utility trade-offs, architectural advantages in model segmentation, and the effectiveness of the “SS-OP + Sketch” mechanism in balancing privacy and representation quality, focusing on a setting with  $\hat{\alpha} = 0.1$ ,  $\mathcal{B}_{\text{eff}} \in [50,100]$  Mbps,  $p = 6$ ,  $q = 4$ ,  $o = 2$ .

**Analysis of System Utility and Communication Efficiency.** Fig. 5 compares ELSA with an uncompressed Vanilla Model (performance upper bound). Despite using only 26–31% of the communication volume ( $3.26 \times$ – $3.78 \times$  less), ELSA achieves competitive performance (e.g., 83.93% on CB and 81.78% on MultiRC), demonstrating that our sketch-based compression preserves essential updates with high fidelity. Furthermore, Table 2 shows ELSA consistently achieves the lowest total communication time to convergence across eight



(a) TC tasks

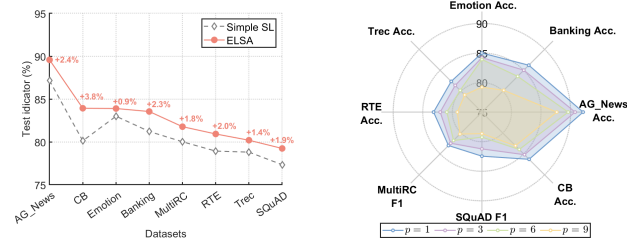
(b) NLI tasks

Figure 5: Evaluation performance and communication reduction of ELSA versus uncompressed schemes on various datasets (Indicator are Acc. (RTE, CB) and F1 (MultiRC, SQuAD), compression ratio  $\rho = 4.2$ ).

datasets. It reduces time by 69.3–73.7% vs. Vanilla and 6.05–12.64% vs. strong baselines (e.g., FedProx, RaSA), with the largest gains on complex tasks like SQuAD (e.g.,  $0.85 \times 10^3$  s faster than RoFed), which indicates that, even under compression, ELSA’s behavior-aware hierarchical clustering scheme maintains superior generalization and robustness compared to other methods. Next, in Table 3, we analyze ELSA’s sensitivity to compression ratio  $\rho$ . Performance peaks at low  $\rho$  (e.g., 92.33% on AG\_News at  $\rho = 2.1$ ) but degrades sharply at high  $\rho$  (e.g., 78.03% at  $\rho = 11.8$ ). Communication benefit grows with  $\rho$  (up to  $4.70 \times$ ), yet excessive compression distorts semantic representations, especially on NLI/QA tasks. We find that  $\rho \in [2.1, 4.2]$  offers the best trade-off, delivering  $1.63 \times$ – $2.57 \times$  communication savings with near-optimal accuracy, while larger  $\rho$  should be reserved for extreme bandwidth constraints.

**Impact of model segmentation.** We conduct a series of sensitivity analyses focusing on model segmentation depth and the effectiveness of our hierarchical aggregation compared to vanilla SL. Firstly, we compare ELSA against simplified SL (Simple SL), where clients interact directly with the cloud server, without KLD clustering or hierarchical aggregation, using the same model partition ( $p = 6, q = 4, o = 2$ ) and sketch-based compression. As shown in Fig. 6(a), ELSA achieves an average performance improvement ranging from +1.4% to +3.8% across various datasets. This gain demonstrates that our design, by incorporating KLD-based client clustering and multi-attribute weighted aggregation effectively mitigates the intrinsic limitations of SL. Next, we evaluate ELSA with varying client-side depth  $p \in \{1, 3, 6, 9\}$  (with  $(q, o) = (9, 2), (7, 2), (4, 2), (1, 2)$  to keep the total number of transformer blocks at 12,  $o = 2$  is fixed as it does not affect trends). As shown in Fig. 6(b), performance drops sharply when  $p \geq 6$ . This stems from over-personalization: deeper local training causes the feature extractor to overfit to non-IID client data, degrading its ability to learn universal semantics. Our results suggest keeping  $p < 6$  is sufficient for robust performance.

**Quantitative Analysis of Data Desensitization and Privacy.** Table 4 evaluates the privacy–utility trade-off of SS-OP + Sketch under varying compression ratios. Following [Li *et al.*, 2023; Wan *et al.*, 2024], we consider two threat models: (i) *Reconstruction attacks* by a semi-honest server, measured via cosine similarity (Cos Sim.) and MSE between original and reconstructed hidden states; (ii) *Token identifi-*



(a)

(b)

Figure 6: Left subplot: ELSA vs. Simple SL: a performance comparison; Right subplot: effects of collaborative training schemes on model performance.

Method	$\rho = 2.1$			$\rho = 4.2$			$\rho = 8.4$		
	Cos Sim.	MSE	Token Acc.	Cos Sim.	MSE	Token Acc.	Cos Sim.	MSE	Token Acc.
Direct Transmission	1.0000	0.0000	53.13%	—	—	—	—	—	—
Gaussian Noise	0.9137	0.0617	50.11%	—	—	—	—	—	—
Sketch Only	0.3599	2.1509	4.07%	0.2655	4.1584	1.96%	0.1975	7.0615	1.13%
ELSA ( $r = 8$ )	-0.0334	2.6979	1.21%	-0.0244	4.7059	0.38%	-0.0220	7.7735	0.09%
ELSA ( $r = 16$ )	-0.0167	2.7669	0.45%	-0.0122	4.7046	0.08%	-0.0078	7.7492	0.00%

Note: “—” indicates that the method is independent of the compression ratio  $\rho$  (i.e., no compression is applied).

Table 4: Comparison of privacy and utility metrics under different compression rates  $\rho$ .

cation attacks, evaluated by token recovery accuracy (Token Acc.). We compare against three baselines: Direct Transmission (no protection), Gaussian Noise ( $\mathcal{N}(0, 0.25)$  for DP), and Sketch Only (compression without SS-OP). As shown in Table 4, Direct Transmission is highly vulnerable (Cos Sim. = 1.0, Token Acc. = 53.13%), while Gaussian Noise offers only marginal protection (Cos Sim. = 0.9137). Sketch Only reduces token recovery (e.g., 1.13% at  $\rho = 8.4$ ) but retains exploitable semantic structure, as indicated by its positive cosine similarity. In contrast, ELSA integrates SS-OP with sketching, driving cosine similarity to near or below zero and suppressing token accuracy to near-zero levels. Notably, increasing the semantic subspace dimension from  $r = 8$  to  $r = 16$  further reduces token identification accuracy (e.g., from 0.38% to 0.08% at  $\rho = 4.2$ ) while maintaining similarly low cosine similarity. This suggests that, under appropriate compression ratios, a larger  $r$  enhances privacy by perturbing a richer set of semantic directions without degrading utility. The slight MSE increase over Sketch Only is benign for training, confirming that ELSA achieves strong privacy without sacrificing utility.

## 5 Conclusion

We propose ELSA, a privacy-aware and efficient HFL framework for distributed LLM fine-tuning in heterogeneous, resource-constrained edge environments. By integrating split learning within a hierarchical architecture, ELSA jointly mitigates computational fragmentation, data heterogeneity, and communication overhead. Extensive experiments on eight NLP tasks show that ELSA consistently outperforms state-of-the-art methods in both training efficiency and final model performance. Future work includes scaling ELSA to ultra-large models (e.g., LLaMA- and GPT-scale) and developing adaptive strategies for model splitting and communication compression to dynamically respond to edge resource and network variations.

## References

[Chen *et al.*, 2024] Jiewei Chen, Shaoyong Guo, Qi Qi, Jiakai Hao, Song Guo, and Xuesong Qiu. Enabling Foundation Models: A Distributed Collaboration Framework Based on Graph Federated Learning. *IEEE Trans. Serv. Comput.*, 17(6):3569–3582, 2024.

[Chen *et al.*, 2025a] Haiyang Chen, Xiaolong Xu, Xiang Zhu, Xiaokang Zhou, Fei Dai, Yansong Gao, et al. Where Does This Data Come From? Enhanced Source Inference Attacks in Federated Learning. In *IJCAI*, pages 4815–4823, 2025.

[Chen *et al.*, 2025b] Qian Chen, Zilong Wang, Mengqing Yan, Haonan Yan, Xiaodong Lin, and Jianying Zhou. DeFedGCN: Privacy-Preserving Decentralized Federated GCN for Recommender System. *IEEE Trans. Serv. Comput.*, 18(2):729–742, 2025.

[Chen *et al.*, 2025c] Xiaohong Chen, Guanying Xu, Xuesong Xu, Haichong Jiang, Zhiping Tian, and Tao Ma. Multicenter Hierarchical Federated Learning With Fault-Tolerance Mechanisms for Resilient Edge Computing Networks. *IEEE Trans. Neural Netw. Learn. Syst.*, 36(1):47–61, 2025.

[Cheng *et al.*, 2023] Zhipeng Cheng, Xiaoyu Xia, Minghui Liwang, Xuwei Fan, Yanglong Sun, Xianbin Wang, et al. CHEESE: Distributed Clustering-Based Hybrid Federated Split Learning Over Edge Networks. *IEEE Trans. Parallel Distrib. Syst.*, 34(12):3174–3191, 2023.

[Ding and Hu, 2024] Shengwen Ding and Chenhui Hu. eFedLLM: Efficient LLM Inference Based on Federated Learning. *arXiv preprint arXiv:2411.16003*, 2024.

[Fang *et al.*, 2024] Wenzhi Fang, Dong-Jun Han, Evan Chen, Shiqiang Wang, and Christopher G Brinton. Hierarchical Federated Learning with Multi-Timescale Gradient Correction. In *NeurIPS*, pages 78863–78904, 2024.

[Farr *et al.*, 2025] David Farr, Nico Manzonelli, Iain Cruickshank, and Jevin West. RED-CT: A systems design methodology for using LLM-labeled data to train and deploy edge linguistic classifiers. In *COLING*, pages 58–67, 2025.

[Gao *et al.*, 2022] Liang Gao, Huazhu Fu, Li Li, Yingwen Chen, Ming Xu, and Cheng-Zhong Xu. FedDC: Federated Learning with Non-IID Data via Local Drift Decoupling and Correction. In *CVPR*, pages 10102–10111, 2022.

[Haddadpour *et al.*, 2020] Farzin Haddadpour, Belhal Karimi, Ping Li, and Xiaoyun Li. FedSKETCH: Communication-Efficient and Private Federated Learning via Sketching. *arXiv preprint arXiv:2008.04975*, 2020.

[Kim *et al.*, 2024] Bong-Hyun Kim, Anandakumar Haldorai, and S Suprakash. A Battery Lifetime Monitoring and Estimation Using Split Learning Algorithm in Smart Mobile Consumer Electronics. *IEEE Trans. Consum. Electron.*, 70(3):5942–5951, 2024.

[Li and Roth, 2002] Xin Li and Dan Roth. Learning Question Classifiers. In *COLING*, 2002.

[Li *et al.*, 2020] Tian Li, Anit Kumar Sahu, Manzil Zaheer, Maziar Sanjabi, Ameet Talwalkar, and Virginia Smith. Federated Optimization in Heterogeneous Networks. In *MLSys*, volume 2, pages 429–450, 2020.

[Li *et al.*, 2023] Haoran Li, Mingshi Xu, and Yangqiu Song. Sentence Embedding Leaks More Information than You Expect: Generative Embedding Inversion Attack to Recover the Whole Sentence. In *Findings of ACL*, pages 14022–14040, 2023.

[Liang *et al.*, 2023] Wei Liang, Xiaohong Chen, Suzhen Huang, Guanghao Xiong, Ke Yan, and Xiaokang Zhou. Federal Learning Edge Network Based Sentiment Analysis Combating Global COVID-19. *Computer Communications*, 204:33–42, 2023.

[Lin *et al.*, 2024] Zheng Lin, Guangyu Zhu, Yiqin Deng, Xianhao Chen, Yue Gao, Kaibin Huang, et al. Efficient Parallel Split Learning over Resource-Constrained Wireless Edge Networks. *IEEE Trans. Mobile Comput.*, 23(10):9224–9239, 2024.

[Liu and Zhao, 2026] Chang Liu and Jun Zhao. Enhancing Stability and Resource Efficiency in LLM Training for Edge-Assisted Mobile Systems. *IEEE Trans. Mobile Comput.*, 25(1):1–18, 2026.

[Liu *et al.*, 2022] Haokun Liu, Derek Tam, Mohammed Muqeeth, Jay Mohta, Tenghao Huang, Mohit Bansal, et al. Few-Shot Parameter-Efficient Fine-Tuning is Better and Cheaper than In-Context Learning. In *NeurIPS*, volume 35, pages 1950–1965, 2022.

[Lu *et al.*, 2024] Jianfeng Lu, Yue Chen, Shuqin Cao, Longbiao Chen, Wei Wang, and Yun Xin. LEAP: Optimization Hierarchical Federated Learning on Non-IID Data with Coalition Formation Game. In *IJCAI*, pages 4660–4668, 2024.

[Luo *et al.*, 2025] Haoxiang Luo, Yinqiu Liu, Ruichen Zhang, Jiacheng Wang, Gang Sun, and Dusit Niyato. Toward Edge General Intelligence with Multiple-Large Language Model (Multi-LLM): Architecture, Trust, and Orchestration. *IEEE Trans. Cogn. Commun. Netw.*, 11(6):3563–3585, 2025.

[Ma *et al.*, 2025] Jian Ma, Xincheng Lyu, Jun Jiang, Qimei Cui, Haipeng Yao, and Xiaofeng Tao. SplitFrozen: Split Learning with Device-side Model Frozen for Fine-Tuning LLM on Heterogeneous Resource-Constrained Devices. *arXiv preprint arXiv:2503.18986*, 2025.

[Mai *et al.*, 2024] Zheda Mai, Arpita Chowdhury, Ping Zhang, Cheng-Hao Tu, Hong-You Chen, Vardaan Pahuja, et al. Fine-Tuning is Fine, if Calibrated. In *NeurIPS*, volume 37, pages 136084–136119, 2024.

[McMahan *et al.*, 2017] Brendan McMahan, Eider Moore, Daniel Ramage, Seth Hampson, and Blaise Aguera y Arcas. Communication-Efficient Learning of Deep Networks from Decentralized Data. In *AISTATS*, volume 54, pages 1273–1282, 2017.

[Oluwatobi and Erik, 2020] Olabiyi Oluwatobi and T. Mueller Erik. DLGNet: A Transformer-Based

Model for Dialogue Response Generation. In *Workshop NLP for Conversational AI*, pages 54–62, 2020.

[Qiao *et al.*, 2025] Dewen Qiao, Xiang Ao, Yu Liu, Xuetao Chen, Fuyuan Song, Zheng Qin, et al. Tri-AFLLM: Resource-Efficient Adaptive Asynchronous Accelerated Federated LLMs. *IEEE Trans. Circuits Syst. Video Technol.*, 35(5):4198–4211, 2025.

[Rahad *et al.*, 2025] Md. Rahad, Ruhan Shabab, Mohd. Sultan Ahammad, Md. Mahfuz Reza, Amit Karmaker, and Md. Abir Hossain. KL-FedDis: A Federated Learning Approach with Distribution Information Sharing using Kullback-Leibler Divergence for non-IID Data. *Neuroscience Informatics*, 5(1):100182, 2025.

[Rajpurkar *et al.*, 2016] Pranav Rajpurkar, Jian Zhang, Konstantin Lopyrev, and Percy Liang. SQuAD: 100,000+ Questions for Machine Comprehension of Text. In *NaturIPS*, pages 2383–2392, 2016.

[Sai *et al.*, 2025] Yinghui Sai, Xiaoyi Wu, Jiacheng Jiang, Yuxiang Huang, Qian Yan, Zongpeng Li, et al. Optimizing Hierarchical Federated Learning: A Reinforcement Learning Approach. *IEEE Trans. Consum. Electron.*, 71(2):4076–4086, 2025.

[Tang *et al.*, 2025] Jian Tang, Zhao Huang, and Chunqiang Li. MT-FBERT: Malicious Traffic Detection Based on Efficient Federated Learning of BERT. *Future Internet*, 17(8), 2025.

[Tian and Yuan, 2025] Jiazhao Tian and Yachao Yuan. HFL-FlowLLM: Large Language Models for Network Traffic Flow Classification in Heterogeneous Federated Learning. *arXiv preprint arXiv:2511.14199*, 2025.

[Tian *et al.*, 2022] Yuanyishu Tian, Yao Wan, Lingjuan Lyu, Dezhong Yao, Hai Jin, and Lichao Sun. FedBERT: When Federated Learning Meets Pre-training. *ACM Trans. Intell. Syst. Technol.*, 13(4), 2022.

[Wan *et al.*, 2024] Zhipeng Wan, Anda Cheng, Yinggui Wang, and Lei Wang. Information leakage from embedding in large language models. *arXiv preprint arXiv:2405.11916*, 2024.

[Wang *et al.*, 2019] Alex Wang, Yada Pruksachatkun, Nikita Nangia, Amanpreet Singh, Julian Michael, Felix Hill, Omer Levy, and Samuel R. Bowman. SuperGLUE: A Stickier Benchmark for General-purpose Language Understanding Systems. In *NaturIPS*, pages 3266 – 3280, 2019.

[Wang *et al.*, 2022] Yujia Wang, Lu Lin, and Jinghui Chen. Communication-Efficient Adaptive Federated Learning. In *ICML*, pages 22802–22838, 2022.

[Wang *et al.*, 2023] Zhousheng Wang, Geng Yang, Hua Dai, and Chunming Rong. Privacy-Preserving Split Learning for Large-Scaled Vision Pre-Training. *IEEE Trans. Inf. Forensics Security*, 18:1539–1553, 2023.

[Wang *et al.*, 2025] Lingling Wang, Mei Huang, Zhengyin Zhang, Meng Li, Jingjing Wang, and Keke Gai. RaSA: Robust and Adaptive Secure Aggregation for Edge-Assisted Hierarchical Federated Learning. *IEEE Trans. Inf. Forensics Security*, 20:4280–4295, 2025.

[Wang *et al.*, 2026] Haoyu Wang, Zilong Yin, Bin Chen, Yujie Zeng, Xiyue Yan, Chenyu Zhou, et al. ROFED-LLM: Robust Federated Learning for Large Language Models in Adversarial Wireless Environments. *IEEE Trans. Netw. Sci. Eng.*, pages 1084–1096, 2026.

[Wu *et al.*, 2024] Bibo Wu, Fang Fang, Xianbin Wang, Donghong Cai, Shu Fu, and Zhiguo Ding. Client Selection and Cost-Efficient Joint Optimization for NOMA-Enabled Hierarchical Federated Learning. *IEEE Trans. Wireless Commun.*, 23(10):14289–14303, 2024.

[Xu *et al.*, 2023] Lingling Xu, Haoran Xie, Si-Zhao Joe Qin, Xiaohui Tao, and Fu Lee Wang. Parameter-Efficient Fine-Tuning Methods for Pretrained Language Models: A Critical Review and Assessment. *arXiv preprint arXiv:2312.12148*, 2023.

[Yang *et al.*, 2025a] Jin Yang, Qiong Wu, Zhiying Feng, Zhi Zhou, Deke Guo, and Xu Chen. Quality-of-Service Aware LLM Routing for Edge Computing With Multiple Experts. *IEEE Trans. Mobile Comput.*, 24(12):13648–13662, 2025.

[Yang *et al.*, 2025b] Wenxin Yang, Xingchen Hu, Xiubin Zhu, Rouwan Wu, Witold Pedrycz, Xinwang Liu, et al. FedMPS: Federated Learning in a Synergy of Multi-Level Prototype-Based Contrastive Learning and Soft Label Generation. *IEEE Trans. Neural Netw. Learn. Syst.*, pages 1–1, 2025.

[Yang *et al.*, 2025c] Xiaohong Yang, Minghui Liwang, Liqun Fu, Yuhua Su, Seyyedali Hosseinalipour, Xianbin Wang, and Yiguang Hong. Adaptive UAV-Assisted Hierarchical Federated Learning: Optimizing Energy, Latency, and Resilience for Dynamic Smart IoT. *IEEE Trans. Serv. Comput.*, 18(6):3420–3434, 2025.

[Zhang *et al.*, 2015] Xiang Zhang, Junbo Zhao, and Yann LeCun. Character-Level Convolutional Networks for Text Classification. In *NaturIPS*, page 649–657, 2015.

[Zhang *et al.*, 2025a] Chunjiang Zhang, Gaoyang Shan, Byeong-hee Roh, and Jun Jiang. FM2 Learning: LLM-Based Federated Multi-Task Multi-Domain Learning for Consumer Electronics and IoT Enhancement. *IEEE Trans. Consum. Electron.*, pages 1–1, 2025.

[Zhang *et al.*, 2025b] Mingjin Zhang, Xiaoming Shen, Jian-nong Cao, Zeyang Cui, and Shan Jiang. EdgeShard: Efficient LLM Inference via Collaborative Edge Computing. *IEEE Internet Things J.*, 12(10):13119–13131, 2025.

[Zhou *et al.*, 2025] Liuzhi Zhou, Yu He, Kun Zhai, Xiang Liu, Sen Liu, Xingjun Ma, et al. FedCAda: Adaptive Client-Side Optimization for Accelerated and Stable Federated Learning. In *ICASSP*, pages 1–5, 2025.

## 6 Appendix

### 6.1 Proof of Theorem 1

To analyze the convergence of ELSA, we first note that only the adapter parameters  $\theta$  are trainable, while the pre-trained LLM backbone remains frozen throughout fine-tuning and is thus omitted from the optimization arguments. We then establish convergence under the following standard assumptions [Chen *et al.*, 2025b]:

**Assumption 1** (Lipschitz Smoothness of Local Loss Functions). *There exists  $\mathcal{L} > 0$  such that for each client  $n$  and any parameter vectors  $\theta, \theta'$ ,*

$$\|\nabla F_n(\theta) - \nabla F_n(\theta')\| \leq \mathcal{L} \|\theta - \theta'\|, \quad \forall n, \theta, \theta'. \quad (16)$$

**Assumption 2** (Bounded SGD Variance and non-IID Heterogeneity). *There exist constants  $\sigma_1^2, \sigma_2^2 > 0$  such that*

$$\mathbb{E} [\|\nabla F_n(\theta) - \nabla f_n(\theta; \mathbf{b})\|^2] \leq \sigma_1^2, \quad (\text{Local SGD variance}) \quad (17)$$

$$\left\| \nabla F_n(\theta) - \nabla \tilde{F}(\theta) \right\|^2 \leq \sigma_2^2, \quad (\text{non-IID data heterogeneity}) \quad (18)$$

where  $f_n(\cdot; \mathbf{b})$  denotes the loss on a mini-batch  $\mathbf{b}$  sampled from client  $n$ 's local data, and  $\tilde{F}(\theta) = \frac{1}{N} \sum_{n=1}^N F_n(\theta)$  is the global objective.

**Assumption 3** (Error from Sketching and Median Reconstruction). *The SS-OP transformation is orthogonal and preserves norms and inner products without bias. However, the subsequent hash-based sketching and median-based reconstruction introduce approximation errors. Specifically, the reconstructed hidden state  $\tilde{\mathbf{H}}_n^{\text{up}}$  satisfies:*

$$\left\| \mathbb{E}[\tilde{\mathbf{H}}_n^{\text{up}}] - \mathbf{H}_n^{\text{up}} \right\| \leq \epsilon_{\text{sketch}}, \quad (\text{Bias}) \quad (19)$$

$$\mathbb{E} \left[ \left\| \tilde{\mathbf{H}}_n^{\text{up}} - \mathbb{E}[\tilde{\mathbf{H}}_n^{\text{up}}] \right\|^2 \right] \leq \sigma_{\text{sketch}}^2, \quad (\text{Variance}) \quad (20)$$

where  $\epsilon_{\text{sketch}}$  arises from the bias of the median estimator, and  $\sigma_{\text{sketch}}^2$  accounts for variance due to hashing collisions. The total mean squared error is bounded by  $\delta^2 \triangleq \epsilon_{\text{sketch}}^2 + \sigma_{\text{sketch}}^2$ .

Under Assumption 1, the reconstruction error in hidden states induces a bounded error in the computed gradients. Extending Lemma 1 of [Haddadpour *et al.*, 2020] to the biased setting, the gradient  $\mathbf{g}_n$  computed using the reconstructed states satisfies:

$$\begin{aligned} \mathbb{E} [\|\mathbf{g}_n - \nabla F_n(\theta)\|^2] &\leq \underbrace{\mathbb{E} [\|\nabla f_n(\theta; \mathbf{b}) - \nabla F_n(\theta)\|^2]}_{\leq \sigma_1^2} \\ &\quad + \underbrace{\mathcal{L}^2 \delta^2}_{\text{sketching error}} \triangleq \sigma_{\text{local}}^2. \end{aligned} \quad (21)$$

Here,  $\sigma_{\text{local}}^2$  captures the combined effect of stochastic sampling and sketching-induced noise at each client.

Critically, the non-IID data heterogeneity (Assumption 2) is *not* absorbed into  $\sigma_{\text{local}}^2$ ; instead, it manifests as a systematic deviation between local and global gradients. Let  $\mathbf{r}_g$  denote

the aggregated update direction after client-side computation, compression, and server-side averaging. Then, the total error relative to the true global gradient satisfies:

$$\begin{aligned} \mathbb{E} \left[ \left\| \mathbf{r}_g - \nabla \tilde{F}(\theta_g) \right\|^2 \right] &\leq \frac{1}{N} \sum_{n=1}^N \mathbb{E} [\|\mathbf{g}_n - \nabla F_n(\theta_g)\|^2] \\ &\quad + \frac{1}{N} \sum_{n=1}^N \left\| \nabla F_n(\theta_g) - \nabla \tilde{F}(\theta_g) \right\|^2 \leq \sigma_{\text{local}}^2 + \sigma_2^2. \end{aligned} \quad (22)$$

This decomposition explicitly separates the impact of *local randomness* ( $\sigma_{\text{local}}^2$ ) from *data heterogeneity* ( $\sigma_2^2$ ), ensuring a theoretically sound convergence characterization.

Building upon the above error decomposition, we establish the following convergence guarantee for ELSA.

*Proof.* By Assumption 1 (Lipschitz smoothness of  $\tilde{F}(\cdot)$ ), the following inequality holds for any global iteration  $g$ :

$$\tilde{F}(\theta_{g+1}) \leq \tilde{F}(\theta_g) - \eta \langle \nabla \tilde{F}(\theta_g), \mathbf{r}_g \rangle + \frac{\mathcal{L}\eta^2}{2} \|\mathbf{r}_g\|^2. \quad (23)$$

Taking expectation over the randomness in SGD and sketching, we decompose the update direction as:

$$\mathbb{E}[\mathbf{r}_g] = \nabla \tilde{F}(\theta_g) + \underbrace{\left( \mathbb{E}[\mathbf{r}_g] - \nabla \tilde{F}(\theta_g) \right)}_{\text{zero-mean under unbiased aggregation}}, \quad (24)$$

but more importantly, from the error decomposition in Section III.C, we have:

$$\mathbb{E} \left[ \left\| \mathbf{r}_g - \nabla \tilde{F}(\theta_g) \right\|^2 \right] \leq \sigma_{\text{local}}^2 + \sigma_2^2. \quad (25)$$

We now bound the two key terms in the smoothness inequality.

**(Step 1) Inner product term.** Using the identity  $\mathbb{E}[\langle a, X \rangle] = \langle a, \mathbb{E}[X] \rangle$ , we get:

$$\begin{aligned} -\mathbb{E}[\langle \nabla \tilde{F}(\theta_g), \mathbf{r}_g \rangle] &= -\langle \nabla \tilde{F}(\theta_g), \mathbb{E}[\mathbf{r}_g] \rangle \\ &= -\|\nabla \tilde{F}(\theta_g)\|^2 - \langle \nabla \tilde{F}(\theta_g), \mathbb{E}[\mathbf{r}_g] - \nabla \tilde{F}(\theta_g) \rangle. \end{aligned} \quad (26)$$

Applying Cauchy-Schwarz and Young's inequality ( $ab \leq \frac{a^2}{2} + \frac{b^2}{2}$ ):

$$-\langle \nabla \tilde{F}(\theta_g), \mathbb{E}[\mathbf{r}_g] - \nabla \tilde{F}(\theta_g) \rangle \leq \|\nabla \tilde{F}(\theta_g)\| \cdot \|\mathbb{E}[\mathbf{r}_g] - \nabla \tilde{F}(\theta_g)\| \leq \frac{1}{2} \|\nabla \tilde{F}(\theta_g)\|^2 + \frac{1}{2} \|\mathbb{E}[\mathbf{r}_g] - \nabla \tilde{F}(\theta_g)\|^2. \quad (27)$$

Note that by Jensen's inequality,

$$\|\mathbb{E}[\mathbf{r}_g] - \nabla \tilde{F}(\theta_g)\|^2 \leq \mathbb{E}[\|\mathbf{r}_g - \nabla \tilde{F}(\theta_g)\|^2] \leq \sigma_{\text{local}}^2 + \sigma_2^2.$$

Thus,

$$-\mathbb{E}[\langle \nabla \tilde{F}(\theta_g), \mathbf{r}_g \rangle] \leq -\frac{1}{2} \|\nabla \tilde{F}(\theta_g)\|^2 + \frac{1}{2} (\sigma_{\text{local}}^2 + \sigma_2^2). \quad (28)$$

**(Step 2) Quadratic term.** Using  $\|a + b\|^2 \leq 2\|a\|^2 + 2\|b\|^2$ ,

$$\begin{aligned} \mathbb{E}[\|\mathbf{r}_g\|^2] &= \mathbb{E}[\|\mathbf{r}_g - \nabla \tilde{F}(\theta_g) + \nabla \tilde{F}(\theta_g)\|^2] \\ &\leq 2\mathbb{E}[\|\mathbf{r}_g - \nabla \tilde{F}(\theta_g)\|^2] + 2\|\nabla \tilde{F}(\theta_g)\|^2 \\ &\leq 2(\sigma_{\text{local}}^2 + \sigma_2^2) + 2\|\nabla \tilde{F}(\theta_g)\|^2. \end{aligned} \quad (29)$$

Substituting (Step 1) and (Step 2) into the smoothness inequality:

$$\begin{aligned}
\mathbb{E}[\tilde{F}(\theta_{g+1})] &\leq \tilde{F}(\theta_g) - \eta \left( \frac{1}{2} \|\nabla \tilde{F}(\theta_g)\|^2 - \frac{1}{2} (\sigma_{\text{local}}^2 + \sigma_2^2) \right) \\
&\quad + \frac{\mathcal{L}\eta^2}{2} \left( 2(\sigma_{\text{local}}^2 + \sigma_2^2) + 2\|\nabla \tilde{F}(\theta_g)\|^2 \right) \\
&= \tilde{F}(\theta_g) - \left( \frac{\eta}{2} - \mathcal{L}\eta^2 \right) \|\nabla \tilde{F}(\theta_g)\|^2 \\
&\quad + \frac{\eta}{2} (\sigma_{\text{local}}^2 + \sigma_2^2) + \mathcal{L}\eta^2 (\sigma_{\text{local}}^2 + \sigma_2^2). \quad (30)
\end{aligned}$$

Choose learning rate  $\eta = \frac{1}{\mathcal{L}\sqrt{G}}$ . For  $G \geq 4$ , we have  $\mathcal{L}\eta \leq \frac{1}{2}$ , so  $\frac{\eta}{2} - \mathcal{L}\eta^2 \geq \frac{\eta}{4}$ . Rearranging:

$$\frac{\eta}{4} \|\nabla \tilde{F}(\theta_g)\|^2 \leq \tilde{F}(\theta_g) - \mathbb{E}[\tilde{F}(\theta_{g+1})] + \left( \frac{\eta}{2} + \mathcal{L}\eta^2 \right) (\sigma_{\text{local}}^2 + \sigma_2^2). \quad (31)$$

Summing over  $g = 0$  to  $G - 1$  and taking total expectation:

$$\begin{aligned}
\frac{\eta}{4} \sum_{g=0}^{G-1} \mathbb{E}[\|\nabla \tilde{F}(\theta_g)\|^2] &\leq \tilde{F}(\theta_0) - \tilde{F}(\theta_G) + G \left( \frac{\eta}{2} + \mathcal{L}\eta^2 \right) (\sigma_{\text{local}}^2 + \sigma_2^2) \\
&\leq \tilde{F}(\theta_0) - \tilde{F}^* + G \left( \frac{\eta}{2} + \mathcal{L}\eta^2 \right) (\sigma_{\text{local}}^2 + \sigma_2^2). \quad (32)
\end{aligned}$$

where  $\tilde{F}^* = \min_{\theta} \tilde{F}(\theta)$ . Then, dividing both sides by  $\frac{\eta}{4}G$ :

$$\begin{aligned}
\frac{1}{G} \sum_{g=0}^{G-1} \mathbb{E}[\|\nabla \tilde{F}(\theta_g)\|^2] &\leq \frac{4(\tilde{F}(\theta_0) - \tilde{F}^*)}{\eta G} + \\
&\quad 4 \left( \frac{1}{2} + \mathcal{L}\eta \right) (\sigma_{\text{local}}^2 + \sigma_2^2) \\
&= \frac{4\mathcal{L}(\tilde{F}(\theta_0) - \tilde{F}^*)}{\sqrt{G}} + 4 \left( \frac{1}{2} + \frac{1}{\sqrt{G}} \right) (\sigma_{\text{local}}^2 + \sigma_2^2). \quad (33)
\end{aligned}$$

For sufficiently large  $G$  (e.g.,  $G \geq 4$ ),  $\frac{1}{\sqrt{G}} \leq \frac{1}{2}$ , so  $\frac{1}{2} + \frac{1}{\sqrt{G}} \leq 1$ . Thus,

$$\frac{1}{G} \sum_{g=0}^{G-1} \mathbb{E}[\|\nabla \tilde{F}(\theta_g)\|^2] \leq \frac{4\mathcal{L}(\tilde{F}(\theta_0) - \tilde{F}^*)}{\sqrt{G}} + \frac{\sigma_{\text{local}}^2}{\sqrt{G}} + \sigma_2^2, \quad (34)$$

where we absorb constants into the  $\sigma_{\text{local}}^2/\sqrt{G}$  term for clarity (since  $\sigma_{\text{local}}^2$  already includes problem-dependent constants). This matches the bound in Theorem 1, completing the proof.  $\square$

**Remark 1.** Theorem 1 shows ELSA converges to a neighborhood of a stationary point at rate  $\mathcal{O}(1/\sqrt{G})$ . Although  $\mathcal{O}(1/G)$  non-IID bias reduction is possible under idealized settings (e.g., single-step updates and unbiased aggregation), our multi-round client-edge collaboration, model splitting, and compression introduce a persistent bias between the expected update and the true gradient. This results in a non-vanishing residual error  $\sigma_2^2$ . In contrast, sketching and SGD noise ( $\sigma_{\text{local}}^2$ ) vanish with training. Convergence is ensured by bounding intra-cluster semantic heterogeneity via KLD-based clustering, which aligns local SS-OP bases  $\{\mathbf{U}_n\}$  and controls aggregation bias.